ACS MATERIALS Au
AN OPEN ACCESS JOURNAL OF THE AMERICAN CHEMICAL SOCIETY



pubs.acs.org/materialsau
Article

# CVD Grown Sub 10 nm Size g-$C_3N_4$ Particle-Decorated $TiO_2$ Nanotube Array Composites for Enhanced Photocatalytic $H_2$ Production

Kosei Ito,* Sho Yoneyama, Shusuke Yoneyama, Paul Fons, and Kei Noda*

Cite This: ACS Mater. Au 2025, 5, 299−307
Read Online



**ABSTRACT:** $TiO_2$ nanotube arrays (NTA) have attracted much attention among photocatalysts because of their large specific surface area and easy surface transfer of excited electrons, and in recent years, attempts have been made to further improve their properties by forming Z-schemes when they are composited with other photocatalysts. However, as the spacing within and between nanotubes is only a few nanometers, the formation of heterojunctions is extremely difficult when $TiO_2$−NTA is composited with other photocatalytic materials with larger grain sizes. Creating nanoparticle photocatalysts with dimensions smaller than those of the nanotube system is thus required to effectively form heterojunctions. We have constructed an original vacuum chemical vapor deposition (CVD) system with fine temperature control, an attribute that we believe is necessary for the preparation of small nanoparticles. Using this system, it is possible to greatly reduce the polymerization rate of melamine, the precursor of the carbon nitride (g-$C_3N_4$) photocatalyst, which offers the benefits of increased reduction power and a metal-free composition. As a result, g-$C_3N_4$ small nanoparticles with particle sizes of about 10 nm were successfully prepared, and heterojunctions could be formed even inside $TiO_2$−NTA. The fabricated $TiO_2$−NTA/g-$C_3N_4$ composite structure exhibited significantly improved redox power and photocatalytic hydrogen production compared to $TiO_2$−NTA and g-$C_3N_4$ alone. In addition, while the hydrogen production rates for $TiO_2$−NTA and g-$C_3N_4$ were almost constant, $TiO_2$−NTA/g-$C_3N_4$ showed a rapid increase in the hydrogen production rate after a certain period of light irradiation, which was presumably caused by oxygen desorption from g-$C_3N_4$. The results of this study provide a method for supporting small nanoparticle materials on nanotube substrates and their importance in improving photocatalytic properties, and will also make a significant contribution not only to the field of photocatalysis but also to other fields requiring small nanoparticle materials.

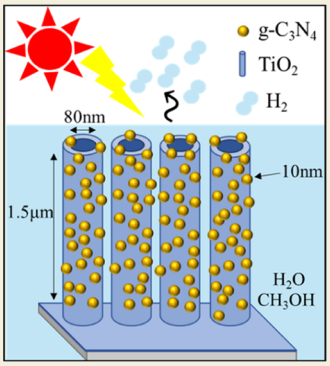


**KEYWORDS:** *$TiO_2$ nanotube arrays, carbon nitride, chemical vapor deposition, small nanoparticles, photocatalyst*

## 1. INTRODUCTION

Titanium dioxide ($TiO_2$) photocatalysis has been studied by many researchers since it was reported by Honda et al. in 1972.[1] Among $TiO_2$ photocatalysts, $TiO_2$ nanotube arrays (NTA) have attracted much attention because of their large specific surface area and easy surface transfer of excited electrons (Figure 1a).[2] In addition, NTA is a substrate material and can be used for a wide range of practical applications. Recently, attempts to improve the performance of $TiO_2$−NTA have been carried out by combining $TiO_2$−NTA with other materials to enhance both the reduction power and spatial separation of electron−hole pairs, which have been weak points of $TiO_2$−NTA.[3,4] This form of composite photocatalysts with enhanced oxidation and reduction power is widely known as Z-scheme photocatalysts, and the key to an efficient Z-scheme system is the formation of appropriate heterojunctions. Photocatalysts with strong reducing power, such as $Cu_2O$,[5] CdS,[6] and g-$C_3N_4$,[7] have been investigated in combination with $TiO_2$−NTA. In this study, we attempted to complex g-$C_3N_4$ (which can be synthesized semipermanently, inexpensively, and easily) with $TiO_2$−NTA.

Initially, $TiO_2$−NTA was heated with melamine (a precursor of g-$C_3N_4$) in the same crucible. After growth, a g-$C_3N_4$ film was found to have covered the $TiO_2$−NTA, as shown in Figure 1b. The experiment was then carried out again with a large reduction in the amount of melamine in the crucible, but a heterogeneous composite was synthesized with a thin film and large g-$C_3N_4$ particles on top of the $TiO_2$−NTA (Figure 1c). This is not favorable for the formation of heterojunctions, which are key to Z-scheme photocatalysis and have been found to be a common problem in other previous studies.[8] One way to overcome these problems is to thermally dissociate the g-$C_3N_4$ powder into small nanoparticles and support the small nanoparticles on $TiO_2$−NTA.[9] However, the thermal dissoci-

Received: August 16, 2024
Revised: November 6, 2024
Accepted: November 25, 2024
Published: December 9, 2024

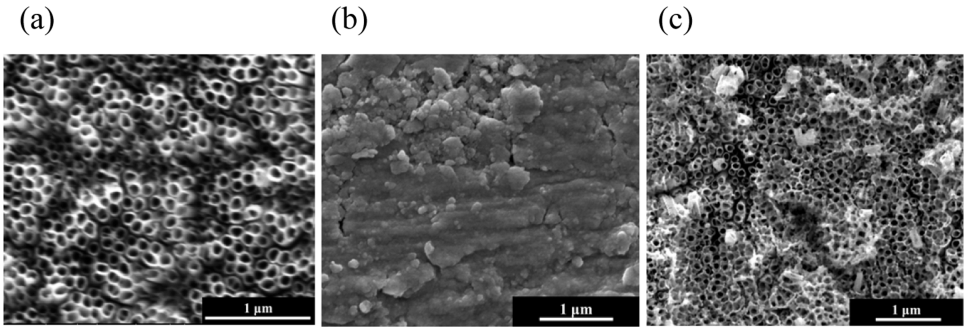


**Figure 1.** (a) SEM image of the as-grown $TiO_2$−NTA. (b) The SEM image of $TiO_2$−NTA/g-$C_3N_4$ synthesized by heating melamine (2 g) and $TiO_2$−NTA in the same crucible. (c) The SEM image of $TiO_2$−NTA/g-$C_3N_4$ synthesized by heating melamine (0.1 g) and $TiO_2$−NTA in the same crucible.

ation process leads to defects and amorphization of the original g-$C_3N_4$ material. In addition, physical vapor deposition is undesirable because it weakens the adhesion of the film to the substrate.

To solve the above problems, it is essential to create pure small nanoparticles of g-$C_3N_4$, which can enter into nanotube apertures of several tens of nanometers in diameter; it is desirable to combine them using a simple deposition method. Thus, we focused on chemical vapor deposition (CVD) apparatus. The main role of the CVD apparatus is to deposit films on devices. In fact, in previous research using a CVD apparatus to combine g-$C_3N_4$ with $TiO_2$−NTA, a g-$C_3N_4$ film was coated onto $TiO_2$−NTA.[10] In this work, to combine g-$C_3N_4$ in the form of small nanoparticles with $TiO_2$−NTA, we constructed an original CVD apparatus (Figure 2) that

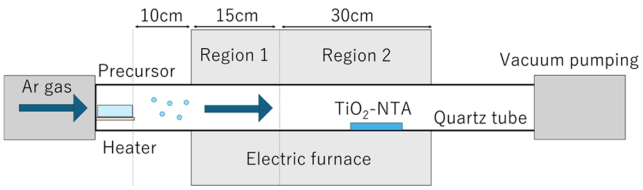


**Figure 2.** Schematic diagram of the original CVD system.

incorporated the following two new features. The first is that the temperature can be adjusted by heaters in regions 1 and 2, allowing the precursor (melamine) to be heated rather than the target material being reheated. This makes it possible to intentionally manipulate the thermal polymerization process from melamine to g-$C_3N_4$, thus allowing for chemical complexation with $TiO_2$−NTA during the thermal polymerization process, preventing the formation of nitrogen defects or amorphization, controlling particle size during transport to the substrate, and overall simplification of the synthesis process. The second feature is that deposition is usually carried out at atmospheric pressure, but our system is evacuated to a pressure of 40−133 Pa. The resulting increase in mean-free path enables ultrasmall state particles to penetrate into the nanotubes because it suppresses polymerization caused by collisions of gas molecules during vapor transport. Furthermore, if the number of particles adsorbed on $TiO_2$−NTA can be controlled, excessive thermal polymerization after adsorption can be prevented and the g-$C_3N_4$ can be deposited as particles rather than films. Also, the low-pressure conditions aid in the formation of highly pure particles and facilitate the formation of heterojunctions with $TiO_2$−NTA.

In this article, we first present the conditions for the synthesis of g-$C_3N_4$ small nanoparticles from melamine using the modified CVD system. Next, observations of the interface between $TiO_2$−NTA and g-$C_3N_4$ small nanoparticles are discussed. Finally, the function of the combined $TiO_2$−NTA/g-$C_3N_4$ as a Z-scheme photocatalyst is evaluated by the redox power and photocatalytic $H_2$ production. Although the current study demonstrates how to composite small nanoparticle photocatalysts into nanotubular substrate photocatalysts and their importance in improving photocatalytic properties, the results of this study are expected to contribute more broadly to not only the field of photocatalysis but also to other fields that require small nanoparticles.

## 2. EXPERIMENTAL METHODS

### 2.1. Materials and Reagents

In this study, the following chemicals and reagents were purchased and used without any further purification: ethylene glycol ($C_2H_6O_2$, Nacalai Tesque; >99.5%), ammonium fluoride ($NH_4F$, Nacalai Tesque; >98%), titanium foil (Ti, Japan Metal Service; >99.5%), 2-propanol ($C_3H_8O$, Nacalai Tesque; >99.7%), melamine ($C_3H_6N_6$, Tokyo Chemical Industry; >98%), terephthalic acid (TA, $C_8H_6O_4$, Nacalai Tesque; >98%), sodium hydroxide (NaOH, Nacalai Tesque; 5 M), 5,5-dimethyl-1-pyrroline-*N*-oxide (DMPO, C6H11NO, Tokyo Chemical Industry; >97%), and methanol ($CH_3OH$, Nacalai Tesque; >99.5%).

### 2.2. Preparation of $TiO_2$−NTA by the Anodic Oxidation Method[11]

The electrolyte was prepared by stirring ethylene glycol (100 mL), ammonium fluoride (0.559 g), and $H_2O$ (11 mL) for 30 min. Next, the anode (titanium foil, 2.5 cm × 3.0 cm) and cathode (platinum foil) were immersed in the prepared electrolyte and a 40 V DC was applied for 1.5 h at room temperature. After application, the samples were immersed in 2-propanol for 30 min for washing. Finally, the washed sample was annealed at 400 °C for 1 h, followed by annealing at 500 °C for 3 h for crystallization.

### 2.3. Support of g-$C_3N_4$ Small Nanoparticles on $TiO_2$−NTA Using CVD

First, melamine (2.0 g) was added to a quartz cell (12.5 mm × 12.5 mm × 45 mm) mounted on a heater in the CVD apparatus, and a $TiO_2$−NTA substrate was placed in region 2. Next, the pressure in the CVD apparatus was lowered to about 40−133 Pa and a 1.5 CCM Ar gas flow was established. Finally, the melamine was heated to 300 °C. 300 °C is the temperature at which melamine begins to sublimate in the thermal polymerization process. The heating ramp time was set to 20 min and held for 10 min. The heating conditions for g-$C_3N_4$ deposition in the tube furnace were set to have a variable temperature in region 1 and a constant temperature of 500 °C in region 2. Region 2 was set to 500 °C because the thermal polymerization temperature


https://doi.org/10.1021/acsmaterialsau.4c00084
ACS Mater. Au 2025, 5, 299−307

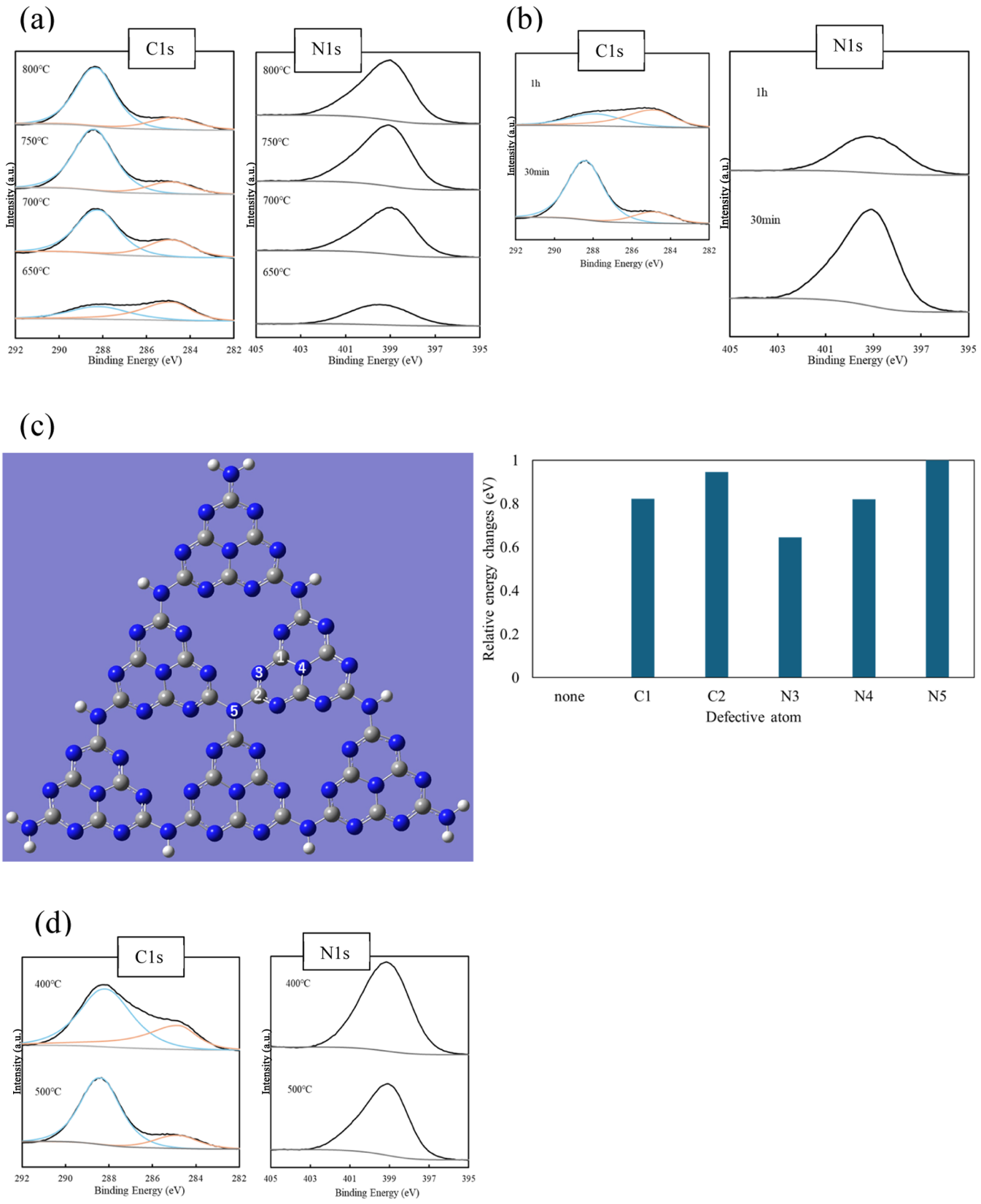


**Figure 3.** (a) XPS spectra of g-$C_3N_4$ deposited on a $TiO_2$−NTA substrate for different region 1 temperatures of the CVD apparatus. (b) XPS spectra of g-$C_3N_4$ deposited on a $TiO_2$−NTA substrate at different holding times when the region 1 temperature of the CVD apparatus was set to 750 °C. (c) Model of the g-$C_3N_4$ structure optimized by quantum chemical calculations and simulated defect formation free energy changes for each carbon or nitrogen atom. (The calculation conditions are described in the Supporting Information). (d) XPS spectra of g-$C_3N_4$ deposited on $TiO_2$−NTA substrates for different temperatures in region 2 of the CVD apparatus.



https://doi.org/10.1021/acsmaterialsau.4c00084
ACS Mater. Au 2025, 5, 299−307

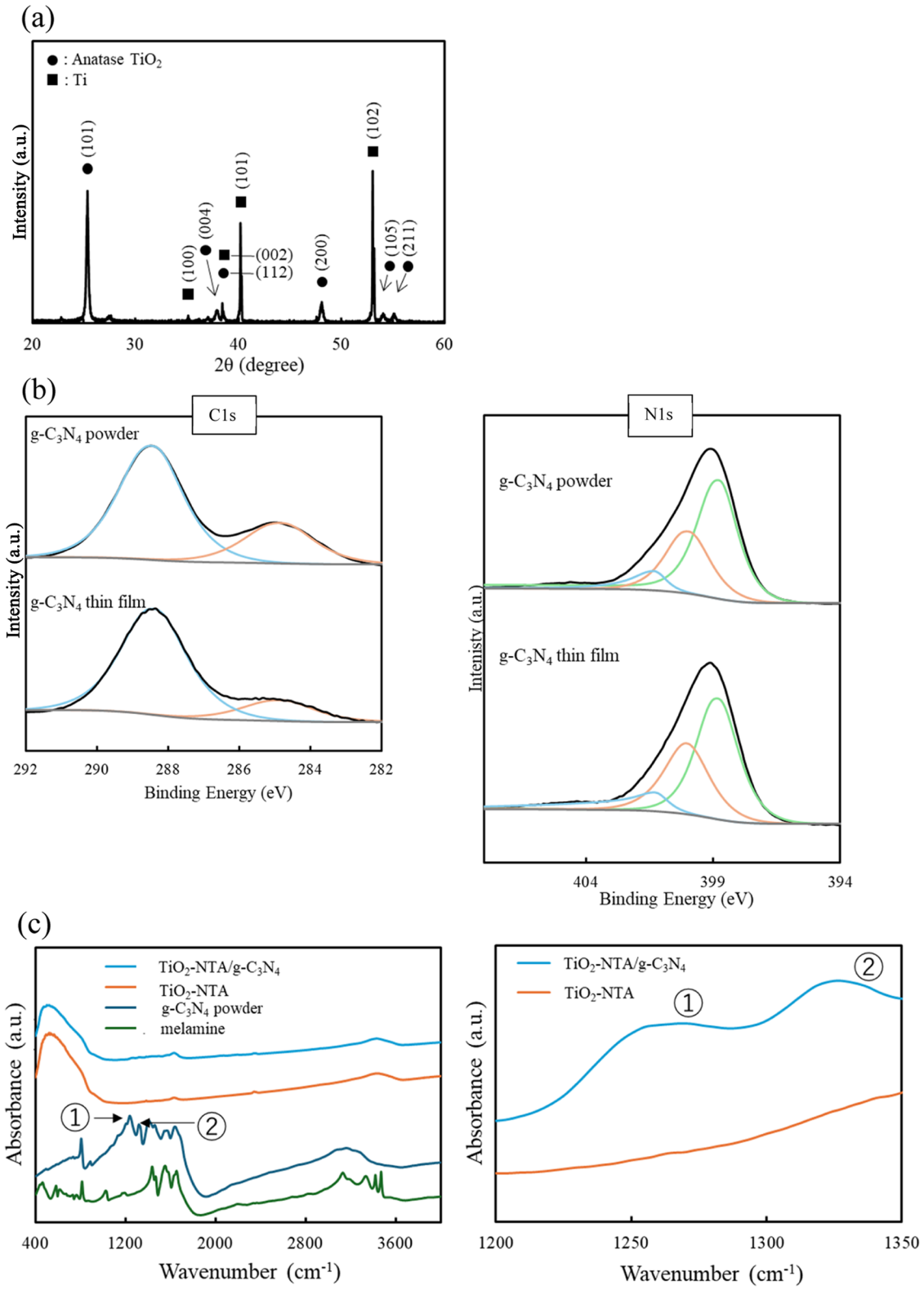


**Figure 4.** (a) XRD spectrum of $TiO_2$−NTA/g-$C_3N_4$. (b) XPS spectra of $TiO_2$−NTA/g-$C_3N_4$ prepared under optimal conditions and g-$C_3N_4$ prepared by the simple heating of powder. (c) FT-IR spectra of melamine, g-$C_3N_4$ powder, $TiO_2$−NTA, and $TiO_2$−NTA/g-$C_3N_4$, and a magnified view of the 1200−1350 $nm^{-1}$ wavenumber region.

of g-$C_3N_4$ is generally 500 °C and the stability limit of $TiO_2$−NTA is 500 °C. The heating ramp times for regions 1 and 2 were set to be 30 min for heating followed by 30 min of constant temperature. The heating of the region 1 heater was initiated when the temperature in region 2 reached 500 °C.

## 2.4. Equipment Used for Materials Characterization

The morphology of the samples was investigated by using a scanning electron microscope (SEM, JSM-7600F, JEOL). Fine structure observation for $TiO_2$−NTA/g-$C_3N_4$ was carried out using a transmission electron microscope (TEM) (Tecnai Osiris, FEI).


https://doi.org/10.1021/acsmaterialsau.4c00084
ACS Mater. Au 2025, 5, 299−307

Chemical state and bonding information were obtained using X-ray photoelectron spectroscopy (XPS, JPS-9010TR, JEOL) with Mg K$\alpha$ radiation and Fourier transform infrared spectroscopy (FT-IR) (ALPHA, Bruker). The crystal structure was investigated by using an X-ray diffractometer (XRD, D8 ADVANCE, Bruker) with Cu−K$\alpha$ radiation. To explore the detailed energy band structure, diffuse-reflectance ultraviolet−visible (UV−vis) absorption spectra were monitored by using a UV−vis-near-infrared (UV−vis-NIR) spectrophotometer (UV-3600Plus, Shimadzu). In addition, the flat band (FB) potential was determined by Mott−Schottky analysis with an electrochemical impedance analyzer (VersaSTAT3, AMETEK). For electrochemical impedance (EI) measurements, a 0.5 M $Na_2SO_4$ aqueous solution was employed as a liquid electrolyte, and Ag/AgCl and platinum wires were used as reference and counter electrodes, respectively. The light source was a xenon lamp (MAX-303, Asahi Spectra, 300 $\leq \lambda \leq$ 600 nm, 500 W/cm$^2$).

### 2.5. Photocatalyst Experiment

The oxidation potential of the photocatalytic material was evaluated from a qualitative assessment based on the amount of OH radicals produced using photoluminescence measurements (PL). First, 100 mL of pure water, 0.083 g of TA, and 0.2 mL of NaOH were added to a 100 mL beaker and stirred for 1 h. Next, 10 mL of the prepared solution was added to a 50 mL beaker, and a substrate sample cut into 2 cm × 1.5 cm was immersed and irradiated with UV−vis light (300 nm $\leq \lambda \leq$ 600 nm) for 15 min. Finally, the solution was placed in a 3 mL quartz cell, and the fluorescence spectrum was measured with a fluorescence spectrophotometer (RF-6000, Shimadzu). The excitation and emission wavelengths were 315 and 425nm for 2-hydroxyterephthalic acid (TAOH), respectively.[12]

The reducing power of the photocatalytic material was evaluated from a qualitative evaluation of the generated reactive oxygen species (ROS) by using electron spin resonance (ESR). First, 5 mL of $CH_3OH$ and 5 mg of DMPO were added to a small container and stirred. Next, the substrate sample was immersed and irradiated with UV−vis light (300 $\leq \lambda \leq$ 600 nm) for 15 min. Finally, the spectra of the ROS were analyzed by using ESR spectroscopy (E-500, Bruker).

A small cell with a quartz window at the top was attached to the original closed system, and a gas chromatograph (GC, GC-8A, Shimadzu) connected to the closed system was used to detect photocatalytic $H_2$ production. First, 6.4 mL of pure water and 1.6 mL of methanol were added to the small cell, and the mixture was stirred. Next, a photocatalyst sample was added to the cell; the lid was closed, and the entire closed system was filled with nitrogen gas. Finally, the system was irradiated by UV−vis light (300 nm $\leq \lambda \leq$ 600 nm), and the $H_2$ production was measured every hour for 5 h.

## 3. RESULTS AND DISCUSSION

### 3.1. Evaluation of Synthesized $TiO_2$ Nanotube Arrays

Figure S1a shows an X-ray diffraction pattern (XRD) that indicates that the Ti substrate was oxidized to anatase $TiO_2$ by anodic oxidation.[13] Furthermore, the XRD patterns shown in Figures 1a and S1b, along with microscopy observations, demonstrate that the synthesized $TiO_2$ forms NTA with an orientation perpendicular to the substrate with a diameter of about 80 nm and a depth of about 1.5 $\mu$m. From the Mott−Schottky (Figure S2a) and Tauc plots (Figure S2b), the CB and VB of the $TiO_2$−NTA were estimated to be 0.1 and 3.4 V (vs normal hydrogen electrode (NHE)), respectively.[14−17]

### 3.2. Synthesis and Evaluation of g-$C_3N_4$ Small Nanoparticles by CVD Method and Their Support on $TiO_2$−NTA

XPS spectra of g-$C_3N_4$ deposited on a $TiO_2$−NTA substrate when the temperature in region 1 was set between 650 and 800 °C are shown in Figure 3a. The peak at 288.6 eV is the peak of carbon nitride derived from the bonding of carbon and nitrogen and appears strongly at temperatures above 750 °C.[16,18,19] The peak at 284.6 eV is reported to be due to incomplete polymerization or C═C bonding due to defects, and the peak appeared strongly at 650 and 700 °C.[16,18,20,21] The C/N ratio at 650 °C is C/N = 3:5.83, clearly indicating a large ratio of nitrogen. On the other hand, at 750 °C, the C/N ratio was close to the theoretical value, C/N = 3:4.07, and the peak at 284.6 eV was clearly smaller than at 700 °C and below.[22] It is known that during the thermal polymerization process of melamine to carbon nitride, the end group is removed as ammonia and the content nitrogen decreases.[23] Therefore, when the temperature in region 1 was set below 700 °C, the ratio of nitrogen is thought to have been larger because melamine did not thermally polymerize completely to g-$C_3N_4$. The g-$C_3N_4$ yield was highest when the temperature of region 1 was above 750 °C.

As can be seen in Figure 3b, when the temperature in region 1 was fixed at 750 °C and the holding time was changed from 30 min to 1 h, the peak intensity at 288.6 eV and N 1s clearly decreased, while the peak intensity at 284.6 eV increased. This is thought to be due to the longer holding time breaking unstable bonds between carbon and nitrogen atoms, leading nitrogen to desorb and the formation of a stable C═C bond.[24,25] We have examined the relative defect formation energies in g-$C_3N_4$ for a variety of sites (with density functional theory (DFT)-based quantum chemical calculation) as shown in Figure 3c. These calculations showed that a defect at the N3 site had the lowest formation energy, supporting the above XPS discussion. Details of the calculation process are reported in the Supporting Information.

The XPS spectra for when region 1 was fixed at 750 °C with a holding time of 30 min while region 2 was held at 400 and 500 °C are shown in Figure 3d. When region 2 was 400 °C, a large peak indicating incomplete polymerization appeared at 284.6 eV. This result indicates that thermal polymerization progresses not only during transport but also after deposition on the substrate.

Based on these results, the optimal conditions for synthesizing g-$C_3N_4$ by CVD are with the temperatures in regions 1 and 2 set for 750 and 500 °C, respectively, with a holding time of 30 min.

From the XRD patterns shown in Figures 4a and S1a, it was confirmed that the crystalline phase of $TiO_2$−NTA did not change after CVD. The reason why no peaks corresponding to loaded g-$C_3N_4$ were observed is thought to be due to the small amount of g-$C_3N_4$ loaded.

XPS spectra comparing g-$C_3N_4$ synthesized by CVD and simple g-$C_3N_4$ powder synthesized by the thermal polymerization of melamine are shown in Figure 4b. It can be seen that g-$C_3N_4$ synthesized by CVD and g-$C_3N_4$ formed by the heating of powder lead to similar shapes.

Figure 4c shows the FT-IR spectra of melamine, g-$C_3N_4$ powder, $TiO_2$−NTA, and $TiO_2$−NTA/g-$C_3N_4$. Compared to melamine, g-$C_3N_4$ powder shows a characteristic peak at 1200−1400 cm$^{-1}$, which originates from aromatic C−N groups.[26] The enlarged FT-IR spectrum shows that $TiO_2$−NTA has no peaks between 1200 and 1400 cm$^{-1}$, while $TiO_2$−NTA/g-$C_3N_4$ has a small peak therein. This result confirms that g-$C_3N_4$ is slightly loaded in $TiO_2$−NTA.

### 3.3. Surface Morphology and Band Structure of $TiO_2$−NTA/g-$C_3N_4$

By analysis of SEM images, we compared the grain size of g-$C_3N_4$ deposited on $TiO_2$−NTA/g-$C_3N_4$ (2.0 g) and $TiO_2$−


https://doi.org/10.1021/acsmaterialsau.4c00084
ACS Mater. Au 2025, 5, 299−307

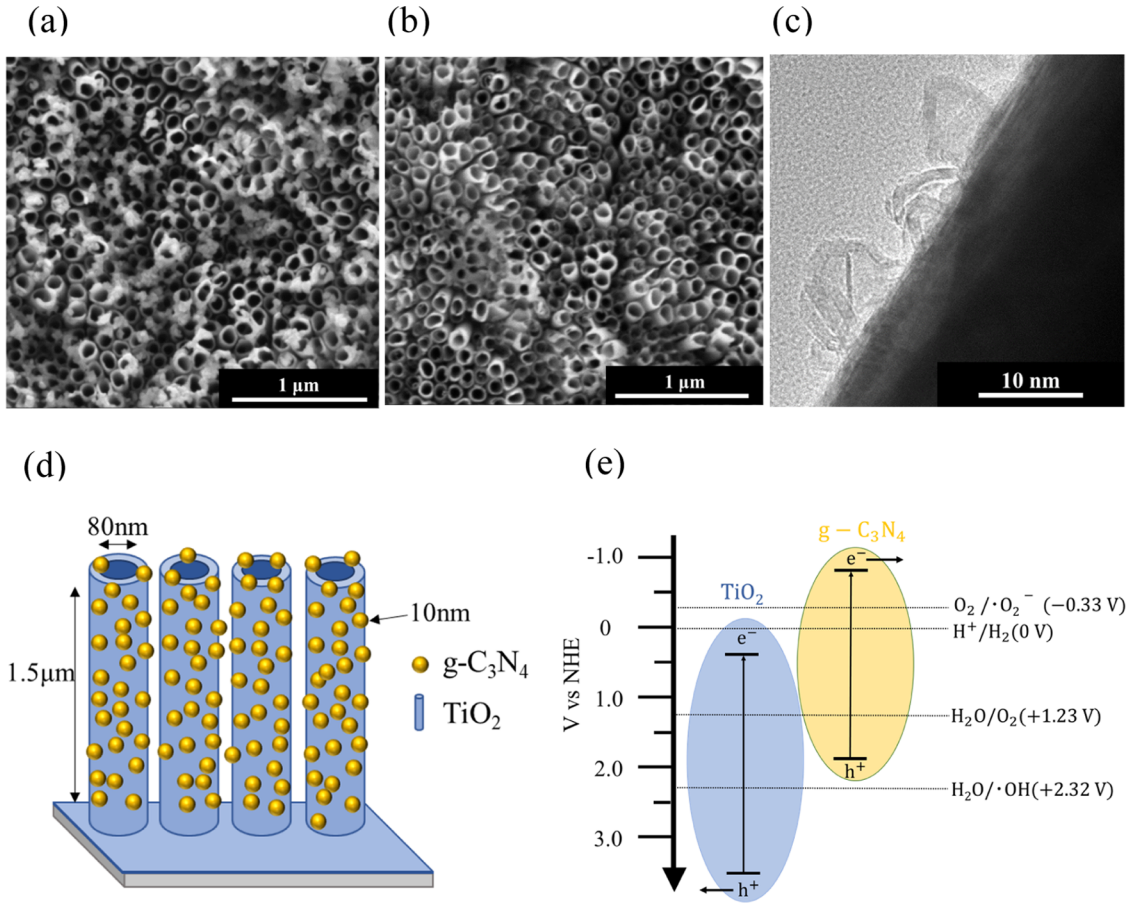


**Figure 5.** (a) SEM image of $TiO_2$−NTA/g-$C_3N_4$ (2.0 g). (b) The SEM image of $TiO_2$−NTA/g-$C_3N_4$ (0.2 g). (c) The TEM image of $TiO_2$−NTA/g-$C_3N_4$ (0.2 g). (d) The schematic diagram of $TiO_2$−NTA/g-$C_3N_4$ (0.2 g) grown by our CVD apparatus. (e) Relative band alignments of $TiO_2$−NTA and g-$C_3N_4$.

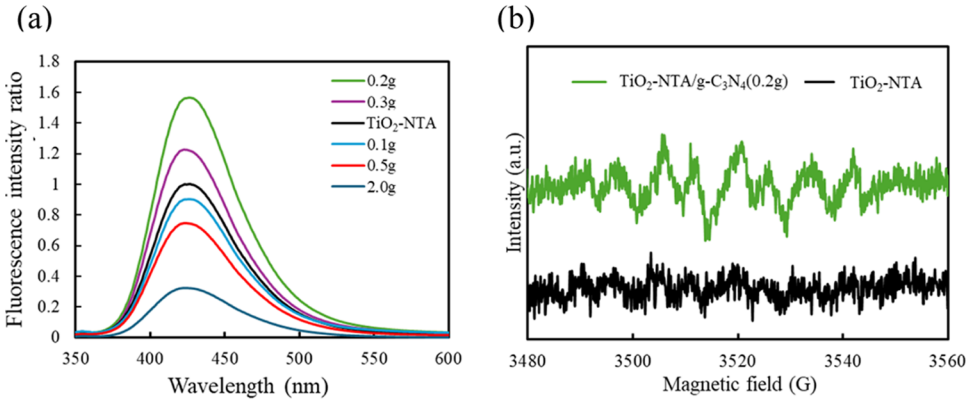


**Figure 6.** (a) PL measurements of $TiO_2$−NTA/g-$C_3N_4$ for varying amounts of melamine placed in the crucible. (b) ESR measurements of $TiO_2$−NTA/g-$C_3N_4$ (0.2 g).

NTA/g-$C_3N_4$ (0.2 g). As shown in Figure 5a, $TiO_2$−NTA/g-$C_3N_4$ (2.0 g) had 30−100 nm of g-$C_3N_4$ deposited on $TiO_2$−NTA. On the other hand, g-$C_3N_4$ was not observed on $TiO_2$−NTA in $TiO_2$−NTA/g-$C_3N_4$ (0.2 g), as shown in Figure 5b. This result contradicts the results of Figures 3 and 4 and implies that g-$C_3N_4$ of $TiO_2$−NTA/g-$C_3N_4$ (0.2 g) is supported on $TiO_2$−NTA as small nanoparticles so that it cannot be observed in the SEM image. Therefore, a more detailed image was obtained by using TEM (Figure 5c). The results show that $TiO_2$−NTA/g-$C_3N_4$ (0.2 g) has evenly spaced g-$C_3N_4$ deposits with a uniform size of about 10 nm on $TiO_2$−NTA. It was also confirmed that the lattice spacing of this g-$C_3N_4$ was 0.34 nm, indicating a 002 peak, which is an interphase stacking of g-$C_3N_4$ (Figure S3).[27] A large amount of melamine was placed in a crucible for the growth of the $TiO_2$−NTA/g-$C_3N_4$ (2.0 g) sample. g-$C_3N_4$ growth of 30 to 100 nm was observed to be nonuniform due to the high molecular density, which facilitated thermal polymerization and aggregation. On the other hand, the $TiO_2$−NTA/g-$C_3N_4$ (0.2 g) sample, which used a smaller amount of melamine, has a lower


https://doi.org/10.1021/acsmaterialsau.4c00084
ACS Mater. Au 2025, 5, 299−307

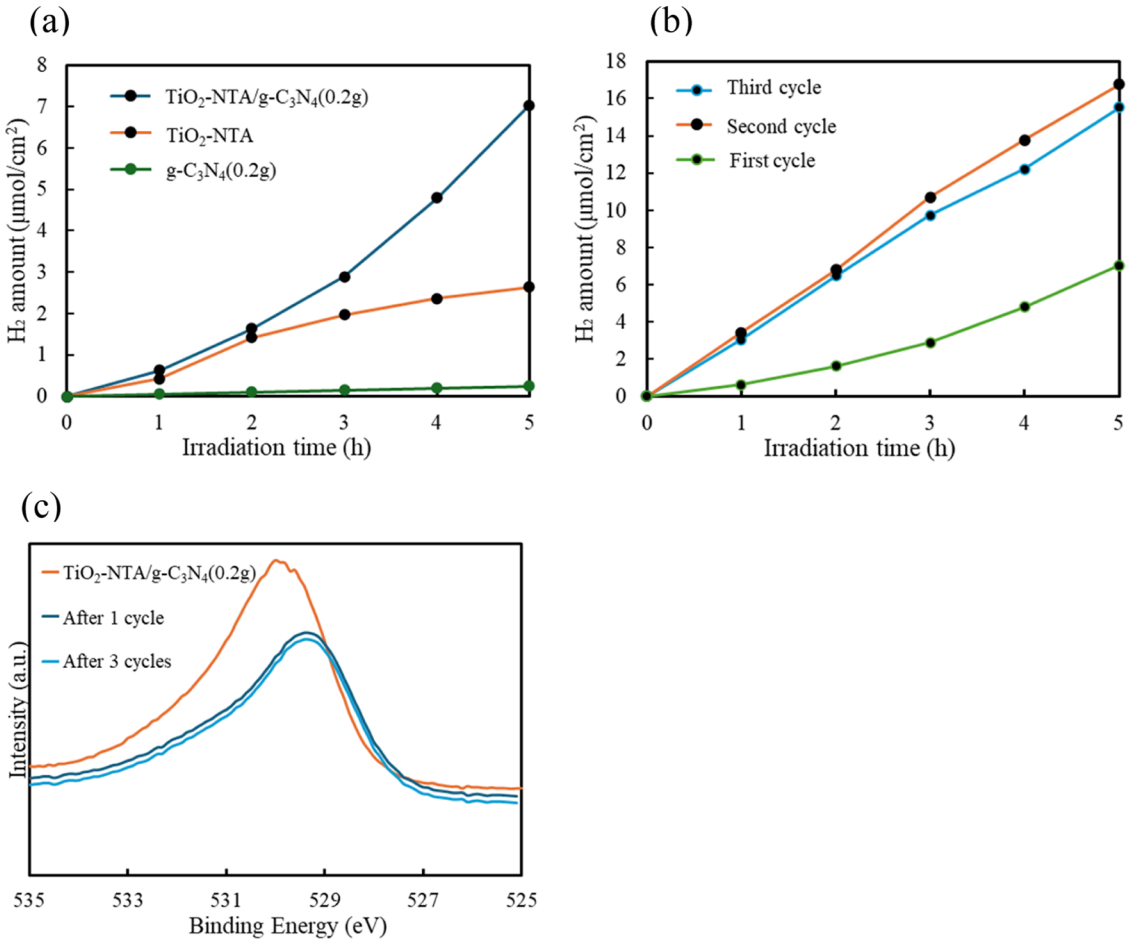


**Figure 7.** (a) Photocatalytic hydrogen production of $TiO_2$−NTA/g-$C_3N_4$ (0.2 g), $TiO_2$−NTA, and g-$C_3N_4$ (0.2 g). (b) Photocatalytic hydrogen production cycling experiment with $TiO_2$−NTA/g-$C_3N_4$ (0.2 g). (c) Change in the XPS O 1s spectra of $TiO_2$−NTA/g-$C_3N_4$ (0.2 g) during a photocatalytic hydrogen production cycling experiment.

molecular density, making polymerization and aggregation less likely to occur and leads to deposition on the $TiO_2$−NTA in the form of uniform small nanoparticles of 10 nm in size. A schematic diagram of the $TiO_2$−NTA/g-$C_3N_4$ (0.2 g) growth process is shown in Figure 5d.

For electrochemical measurements, g-$C_3N_4$ was synthesized on indium tin oxide coated substrates (ITO) by placing them in region 2. From Mott−Schottky (Figure S4a) and Tauc plots (Figure S4b) of g-$C_3N_4$ loaded on ITO, the CB and VB of g-$C_3N_4$ were estimated to be −0.8 and 1.9 V (vs NHE), respectively.[14−17] The band diagrams of $TiO_2$−NTA and g-$C_3N_4$ that are estimated from Figures S2 and S4 are shown in Figure 5e.

### 3.4. Evaluation of the Photocatalytic Redox Power of $TiO_2$−NTA/g-$C_3N_4$ by PL and ESR Measurements

Figure 6a shows the results of a series of PL measurements, where the amount of g-$C_3N_4$ deposited in $TiO_2$−NTA was varied. It can be seen that $TiO_2$−NTA/g-$C_3N_4$(0.2 g) produced the largest number of OH radicals. Figure 6b shows ESR results for $TiO_2$−NTA and $TiO_2$−NTA/g-$C_3N_4$ (0.2 g).[28] No ROS peak was detected for $TiO_2$−NTA, whereas a ROS peak was detected for $TiO_2$−NTA/g-$C_3N_4$ (0.2 g). The band diagram in Figure 5e shows that $TiO_2$−NTA satisfies the formation potential of OH radicals but not that of reactive oxygen species, while g-$C_3N_4$ satisfies the formation potential of reactive oxygen species but not that of OH radicals.[29,30] Therefore, taking into account the results of the PL and ESR measurements, it is concluded that $TiO_2$−NTA/g-$C_3N_4$ (0.2 g) forms a Z-scheme reaction, meaning that efficient charge separation occurred.

### 3.5. Photocatalytic Hydrogen Production by $TiO_2$−NTA/g-$C_3N_4$ (0.2 g)

A comparison of the photocatalytic hydrogen production from methanol aqueous solutions (20%) of $TiO_2$−NTA, g-$C_3N_4$ (0.2 g), and $TiO_2$−NTA/g-$C_3N_4$ (0.2 g) is shown in Figure 7a. $TiO_2$−NTA/g-$C_3N_4$ (0.2 g) generated more $H_2$ than did $TiO_2$−NTA and g-$C_3N_4$ (0.2 g). The band structure of $TiO_2$−NTA does not satisfy the redox potential for generating hydrogen from water, but the reason why it generates a small amount of hydrogen is believed to be due to the band-filling effect.[31] In addition, the results of a cycling experiment in Figure 7b show that $TiO_2$−NTA/g-$C_3N_4$ (0.2 g) produced more $H_2$ in the second cycle than in the first, while the amount of $H_2$ produced in the second and third cycles remained unchanged. On the other hand, there was no significant change in the amount of hydrogen produced by $TiO_2$−NTA in the three cycle experiments (Figure S5). Considering that g-$C_3N_4$ is known as a material that easily adsorbs oxygen and the XPS results in Figure 7c, the first reduction reaction is thought to be a simultaneous proton reduction and adsorbed oxygen reduction.[32,33] After a certain period of time elapses, it is speculated that the adsorbed oxygen desorbs and the excited


https://doi.org/10.1021/acsmaterialsau.4c00084
ACS Mater. Au 2025, 5, 299−307

electrons of g-$C_3N_4$ are active only for proton reduction, suggesting that the photocatalytic hydrogen production in the second reaction was higher than that in the first. The graph in Figure 7b, which shows a change from a nonlinear to a linear increase, confirms the validity of this premise. Previous research has also shown that the initial stage of photocatalytic hydrogen production by g-$C_3N_4$ tends to have a nonlinear increase in the amount of hydrogen produced.[16] The fact that the results of photocatalytic hydrogen production did not change between the second and third cycles indicates that the adsorbed oxygen was lost and that catalytic degradation did not occur. The reason why the hydrogen production of $TiO_2$−NTA alone is linear is thought to be because of the absence of impurities on the $TiO_2$ surface. The oxygen peak in the XPS O 1s spectra of $TiO_2$−NTA measured before and after the cycling experiment (Figure S6) also did not change. Since the O 1s signals in Figure S6 are due to oxygen derived from $TiO_2$, this cycling experiment suggests that $TiO_2$−NTA does not deteriorate even after long-term use. Finally, we confirmed that this reaction was proceeded by photocatalysis (Figure S7).

## 4. CONCLUSIONS

This paper demonstrates that it is possible to uniformly support g-$C_3N_4$ small nanoparticles on nanotube $TiO_2$ by adjusting the temperature and heating time in a CVD apparatus operating at reduced pressure. Furthermore, it was found that $TiO_2$−NTA loaded with g-$C_3N_4$ was more efficient at various photocatalytic properties than $TiO_2$−NTA and g-$C_3N_4$ alone. This indicates that g-$C_3N_4$ small nanoparticles prepared from melamine under CVD conditions function as a semiconductor photocatalyst similar to g-$C_3N_4$ powder prepared by powder heating.

These findings are expected to lead to the development and use of similar CVD apparatuses not only in the field of photocatalysis but also in other fields requiring the support of small nanoparticles.

## ■ ASSOCIATED CONTENT

### Supporting Information

The Supporting Information is available free of charge at https://pubs.acs.org/doi/10.1021/acsmaterialsau.4c00084.

XRD; SEM; Mott−Schottky plot; Tauc plot; TEM; photocatalytic hydrogen production cycling experiment; XPS; and control experiments for photocatalytic $H_2$ generation (PDF)

## ■ AUTHOR INFORMATION


### Corresponding Authors

**Kosei Ito** − *Keio University, Department of Electronics and Electrical Engineering, Yokohama 223-8522, Japan;* orcid.org/0009-0000-3160-5588; Email: itokosei-124183@keio.jp

**Kei Noda** − *Keio University, Department of Electronics and Electrical Engineering, Yokohama 223-8522, Japan;* orcid.org/0000-0003-2031-8975; Email: nodakei@elec.keio.ac.jp

### Authors

**Sho Yoneyama** − *Keio University, Department of Electronics and Electrical Engineering, Yokohama 223-8522, Japan*

**Shusuke Yoneyama** − *Keio University, Department of Electronics and Electrical Engineering, Yokohama 223-8522, Japan*

**Paul Fons** − *Keio University, Department of Electronics and Electrical Engineering, Yokohama 223-8522, Japan;* orcid.org/0000-0002-7820-1924

Complete contact information is available at: https://pubs.acs.org/10.1021/acsmaterialsau.4c00084


### Author Contributions

K.I.: conceptualization, methodology, investigation, writing—original draft, data curation, and writing—review and editing. S.Y.: investigation and data curation. S.Y.: investigation and data curation. P.F.: methodology and writing—review and editing. K.N.: conceptualization, methodology, writing—review and editing, supervision, and project administration.

### Notes

The authors declare no competing financial interest.

## ■ ACKNOWLEDGMENTS

This study was supported by a Grant-in-Aid for Scientific Research (KAKENHI No. 19H02174) of the Japan Society for the Promotion of Science (JSPS). K.I. is very grateful for the support from JST SPRING Grant Number JPMJSP2123.

## ■ REFERENCES


(1) Fujishima, A.; Honda, K. Electrochemical photolysis of water at a semiconductor electrode. *Nature* **1972**, *238* (5358), 37−38.

(2) Ikreedeegh, R. R.; Hossen, M. A.; Tahir, M.; Aziz, A. A. A comprehensive review on anodic $TiO_2$ nanotube arrays (TNTAs) and their composite photocatalysts for environmental and energy applications: Fundamentals, recent advances and applications. *Coord. Chem. Rev.* **2024**, *499*, No. 215495, DOI: 10.1016/j.ccr.2023.215495.

(3) Pandey, B.; Rani, S.; Roy, S. C. A scalable approach for functionalization of $TiO_2$ nanotube arrays with g-$C_3N_4$ for enhanced photo-electrochemical performance. *J. Alloys Compd.* **2020**, *846*, No. 155881, DOI: 10.1016/j.jallcom.2020.155881.

(4) Pourhashem, S.; Duana, J.; Guana, F.; Wanga, N.; Gaoa, Y.; Hou, B. New effects of $TiO_2$ nanotube/g-$C_3N_4$ hybrids on the corrosion protection performance of epoxy coatings. *J. Mol. Liq.* **2020**, *317*, No. 114214, DOI: 10.1016/j.molliq.2020.114214.

(5) Liu, G.; Zheng, F.; Li, J.; Zeng, G.; Ye, Y.; Larson, D. M.; Yano, J.; Crumlin, E. J.; Ager, J. W.; Wang, L. W.; Toma, F. M. Investigation and mitigation of degradation mechanisms in $Cu_2O$ photoelectrodes for $CO_2$ reduction to ethylene. *Nat. Energy* **2021**, *6*, 1124−1132.

(6) Wang, F.; Hou, T.; Zhao, X.; Yao, W.; Fang, R.; Shen, K.; Li, Y. Ordered macroporous carbonous frameworks implanted with CdS quantum dots for efficient photocatalytic $CO_2$ reduction. *Adv. Mater.* **2021**, *33*, No. 2102690, DOI: 10.1002/adma.202102690.

(7) Wang, S.; Zhan, J.; Chen, K.; Ali, A.; Zeng, L.; Zhao, H.; Hu, W.; Zhu, L.; Xu, X. Potassium-doped g-$C_3N_4$ achieving efficient visible-light-driven $CO_2$ reduction. *ACS Sustainable Chem. Eng.* **2020**, *8*, 8214−8222.

(8) Tan, M.; Ma, Y.; Yu, C.; Luan, Q.; Li, J.; Liu, C.; Dong, W.; Su, Y.; Qiao, L.; Gao, L.; Lu, Q.; Bai, Y. Boosting photocatalytic hydrogen production via interfacial engineering on 2D ultrathin Z-scheme $ZnIn_2S_4$ /g-$C_3N_4$ heterojunction. *Adv. Funct. Mater.* **2022**, *32*, No. 2111740, DOI: 10.1002/adfm.202111740.

(9) Li, Y.; Ren, Z.; He, Z.; Ouyang, P.; Duan, Y.; Zhang, W.; Lv, K.; Dong, F. Crystallinity-defect matching relationship of g-$C_3N_4$: Experimental and theoretical perspectives. *Green Energy Environ.* **2024**, *9*, 623−658.

(10) Gao, Z.-D.; Qu, Y.-F.; Zhou, X.; Wang, L.; Song, Y.-Y.; Schmuki, P. Pt-Decorated g-$C_3N_4$/$TiO_2$ Nanotube Arrays with

Enhanced Visible-Light Photocatalytic Activity for $H_2$ Evolution. *ChemistryOpen* **2016**, *5*, 197−200.
(11) Goto, H.; Masegi, H.; Sadale, S. B.; Noda, K. Intricate behaviors of gas phase $CO_2$ photoreduction in high vacuum using $Cu_2O$-loaded $TiO_2$ nanotube arrays. *J. CO2 Util.* **2022**, *59*, No. 101964, DOI: 10.1016/j.jcou.2022.101964.
(12) Sotiles, A. R.; Barbosab, L. V.; Vedovatob, Y. P.; Wypycha, F.; Fariab, E. H. Effect of $Zn_2Cr$ layered double hydroxide on photocatalytic hydroxylation of terephthalic acid and photodegradation of sodium diclofenac. *Catal. Today* **2023**, *423*, No. 114287, DOI: 10.1016/j.cattod.2023.114287.
(13) Sreekantan, S.; Hazan, R.; Lockman, Z. Photoactivity of anatase−rutile $TiO_2$ nanotubes formed by anodization method. *Thin Solid Films* **2009**, *518*, 16−21.
(14) Ito, K.; Uchida, R.; Noda, K. Visible light-assisted hydrogen generation over platinum-loaded tungsten trioxide nanorods with the hexagonal and triclinic phases. *J. Photochem. Photobiol. A* **2023**, *443*, No. 114824, DOI: 10.1016/j.jphotochem.2023.114824.
(15) Zos'ko, N. A.; Aleksandrovsky, A. S.; Kenova, T. A.; Gerasimova, M. A.; Nikolay, G.; Maksimov, N. G.; Taran, O. P. Cyclic voltammetry as an activation method of $TiO_2$ nanotube arrays for improvement of photoelectrochemical water splitting performance. *ChemPhotoChem* **2023**, *7*, No. e202300100, DOI: 10.1002/cptc.202300100.
(16) Ito, K.; Noda, K. Highly efficient hydrogen production and selective $CO_2$ reduction by the $C_3N_5$ photocatalyst using only visible light. *Phys. Chem. Chem. Phys.* **2024**, *26*, 153−160.
(17) Montakhab, E.; Rashchi, F.; Sheibani, S. Enhanced photocatalytic activity of $TiO_2$ nanotubes decorated with Ag nanoparticles by simultaneous electrochemical deposition and reduction processes. *Appl. Surf. Sci.* **2023**, *615*, No. 156332, DOI: 10.1016/j.apsusc.2023.156332.
(18) Liu, Y.; Gaob, Y.; Chena, L.; Lia, L.; Dinga, D.; Daia, Z. MnOx-decorated oxygen-doped g-$C_3N_4$ with enhanced photocatalytic activity for efficient removal of uranium(VI). *Sep. Purif. Technol.* **2023**, *307*, No. 122794, DOI: 10.1016/j.seppur.2022.122794.
(19) Xu, Z.; Chenb, Y.; Wanga, B.; Ranb, Y.; Zhongb, J.; Li, M. Highly selective photocatalytic $CO_2$ reduction and hydrogen evolution facilitated by oxidation induced nitrogen vacancies on g-$C_3N_4$. *J. Colloid Interface Sci.* **2023**, *651*, 645−658.
(20) Ding, Y.; Tang, Y.; Yang, L.; Zeng, Y.; Yuan, J.; Liu, T.; Zhang, S.; Liu, C.; Luo, S. Porous nitrogen-rich carbon materials from carbon self-repairing g-$C_3N_4$ assembled with graphene for high-performance supercapacitor. *J. Mater. Chem. A* **2016**, *4*, 14307−14315.
(21) Feng, P.; Cuia, K.; Haib, Z.; Wang, J.; Wangb, L. Facile synthesis of activated carbon loaded g-$C_3N_4$ composite with enhanced photocatalytic performance under visible light. *Diamond Relat. Mater.* **2023**, *136*, No. 109921, DOI: 10.1016/j.diamond.2023.109921.
(22) Ma, X.; Lv, Y.; Xu, J.; Liu, Y.; Zhang, R.; Zhu, Y. A strategy of enhancing the photoactivity of g-$C_3N_4$ via doping of nonmetal elements: A first-principles study. *J. Phys. Chem. C* **2012**, *116*, 23485−23493.
(23) Wang, X.; Maeda, K.; Thomas, A.; Takanabe, K.; Xin, G.; Carlsson, J. M.; Domen, K.; Antonietti, M. A metal-free polymeric photocatalyst for hydrogen production from water under visible light. *Nat. Mater.* **2009**, *8*, 70−80, DOI: 10.1038/nmat2317.
(24) Liao, J.; Cui, W.; Li, J.; Sheng, J.; Wang, H.; Dong, X.; Chen, P.; Jiang, G.; Wang, Z.; Dong, F. Nitrogen defect structure and $NO^+$ intermediate promoted photocatalytic NO removal on $H_2$ treated g-$C_3N_4$. *Chem. Eng. J.* **2020**, *379*, No. 122282, DOI: 10.1016/j.cej.2019.122282.
(25) Dong, G.; Wen, Y.; Fan, H.; Wang, C.; Cheng, Z.; Zhang, M.; Ma, J.; Zhang, S. Graphitic carbon nitride with thermally-induced nitrogen defects: An efficient process to enhance photocatalytic $H_2$ production performance. *RSC Adv.* **2020**, *10*, 18632−18638.
(26) Pan, Y.; Liu, X.; Zhang, W.; Shao, B.; Liu, Z.; Liang, Q.; Wu, T.; He, Q.; Huang, J.; Peng, Z.; Liu, Y.; Zhao, C. Bifunctional template-mediated synthesis of porous ordered g-$C_3N_4$ decorated with potassium and cyano groups for effective photocatalytic $H_2O_2$ evolution from dual-electron $O_2$ reduction. *Chem. Eng. J.* **2022**, *427*, No. 132032, DOI: 10.1016/j.cej.2021.132032.
(27) Ge, L. Synthesis and photocatalytic performance of novel metal-free g-C3N4 photocatalysts. *Mater. Lett.* **2011**, *65*, 2652−2654.
(28) Yu, Q.; Yang, K.; Li, H.; Li, X. Z-scheme $\alpha$-$Fe_2O_3$/g-$C_3N_4$ with the Fe−OC− bond toward enhanced photocatalytic degradation. *Colloids Surf., A* **2021**, *616*, No. 126269, DOI: 10.1016/j.colsurfa.2021.126269.
(29) Muñoz, E.; Marotti, R.; Navarrete, E. Communication-hydroxyl radicals attack CdTe quantum dots. *J. Electrochem. Soc.* **2021**, *168*, No. 097503, DOI: 10.1149/1945-7111/ac2282.
(30) Zhan, H.; Zhou, Q.; Li, M.; Zhou, R.; Mao, Y.; Wang, P. Photocatalytic $O_2$ activation and reactive oxygen species evolution by surface B-N bond for organic pollutants degradation. *Appl. Catal., B* **2022**, *310*, No. 121329, DOI: 10.1016/j.apcatb.2022.121329.
(31) Diwald, O.; Thompson, T. L.; Goralski, E. G.; Walck, S. D.; Yates, J. T., Jr The effect of nitrogen ion implantation on the photoactivity of $TiO_2$ rutile single crystals. *J. Phys. Chem. B* **2004**, *108*, 52−57.
(32) Wang, X.; Zhang, X.; Wei, Y.; Gao, C.; Bao, J.; Zhang, N. In situ grown $Co_3O_4$ nanosheets in the interlayer space of g-$C_3N_4$ for efficient removal of Hg0 from flue gas. *Fuel* **2022**, *324*, No. 124660, DOI: 10.1016/j.fuel.2022.124660.
(33) Shang, D.; Zhong, Q.; Cai, W. High performance of NO oxidation over Ce-Co-Ti catalyst: The interaction between Ce and Co. *Appl. Surf. Sci.* **2015**, *325*, 211−216.


https://doi.org/10.1021/acsmaterialsau.4c00084
*ACS Mater. Au* 2025, 5, 299−307